MORPHOLOGY OF COLD BARS IN EARLY AND LATE TYPE GALAXIES

A. C. Quillen[1,2]

ABSTRACT

We compare stellar orbits in an early (NGC 4314) and a late-type barred galaxy (NGC 1073). We find that these bars are cold in the sense that the majority of stars can be described as being nearby to periodic orbits. We place limits of $(65\mathrm{km/s})^2$ and $(50\mathrm{km/s})^2$ on the components of the diagonalized velocity dispersion ellipsoid matrix for stars in the bars of NGC 4314 and NGC 1073 respectively. Both bars end near the inner 4:1 Lindblad (ultraharmonic) resonance. We conjecture that a large class of bars end near this resonance. The morphology of the bars depends on the strength of the 4:1 resonance, which is strong in the early-type barred galaxy and weak in the other. This results in a flat bar major axis surface brightness profile for the early-type bar and an exponential profile for the late-type bar.

Subject headings: galaxies: kinematics and dynamics — galaxies: structure — galaxies: spiral

1. Introduction

Many studies of the dynamics of stars in model barred galaxies have concentrated on exploring the structure of periodic orbit families (e.g. Athanassoula 1992a) and the ergodic structure of resonances (Contopoulos & Grosbøl 1989). However, little is known about the actual distribution function of stars in real barred galaxies, or how stars are distributed among the different orbits. One approach is to calculate a library of orbits and iteratively construct a self consistent galaxy model using statistical methods (the Schwarzschild method; Schwarzschild 1979). This approach yields many solutions and has primarily been used to explore the properties of model galaxies (most notably by Pfenniger 1984). Fine structure observed in the images of barred galaxies is not usually present in model or N-body galaxies. This fine structure can exist only in a system with a sufficiently low stellar velocity dispersion. In this paper we place limits on the velocity dispersion in two barred galaxies of different morphology and Hubble type by comparing the properties of their orbits with their shapes.

[1]Astronomy Department, Ohio State University, 174 W. 18th Ave., Columbus, OH 43210

[2]E-mail: quillen@payne.mps.ohio-state.edu

Bars in barred spiral galaxies have been observed to have major axis surface brightness profiles of two forms, either flat or dropping exponentially with increasing distance from the nucleus (Elmegreen & Elmegreen 1985). These two types of barred galaxies can be called exponential-type bars and flat-type bars. Exponential-type bars tend to be in later type galaxies than flat-type bars (Elmegreen et al. 1996). Although there have been a few studies of orbits in individual barred galaxies based upon observations of these galaxies (e.g. Quillen et al. 1994 & Kent & Glaudell 1989), there have been no studies comparing the properties of orbits in different galaxies. In this paper we find the periodic orbits (closed orbits in the frame in which the bar is stationary) in the plane of the galaxy integrated in the gravitational potential of the exponential and late-type barred galaxy NGC 1073. This paper is a continuation of Quillen et al. 1994 (hereafter Paper I) where periodic orbits were found for the flat and early-type barred galaxy NGC 4314. The bar pattern speeds and the disk vertical scale heights are measured. The morphology of the two galaxies and their orbit shapes are compared. We account for the difference in morphology of flat-type and exponential-type bars based on this orbit analysis. We also explore orbits that are nearby the periodic orbits in both galaxies to investigate the effect of the stellar velocity dispersion.

2. The J band image of NGC 1073

NGC 1073 was chosen from the exponential-type bars listed in Elmegreen & Elmegreen 1985. These data are a preliminary part of a survey being carried out at Ohio State University of 200 to 300 galaxies that will produce a library of photometrically calibrated images of late-type galaxies from 0.4 to 2.2μm. For notes on the reduction and observation techniques see Pogge et al. 1996, or for individual examples see Paper I, and Quillen et al. 1995. The galaxy was observed at the 1.8m Perkins Telescope of the Ohio State and Ohio Wesleyan Universities at Lowell Observatory in Flagstaff, AZ using a 256×256 HgCdTe array in the Ohio State Infra-Red Imaging System (OSIRIS) (DePoy et al. 1993). The scale is 1.50 arcsec/pixel.

The J image (see Figure 3b) was used for this study because it has the highest signal to noise of the near infrared images (J, H, and K) included in the survey. A $J-H$ color map reveals no detectable color changes (less than 0.03 mag) across the galaxy suggesting that the mass-to-light ratio is approximately constant across the bar and that the J image is not strongly affected by extinction from star formation or dust. As discussed in Paper I near infrared images are superior to visible images for dynamical studies because of their reduced sensitivity to extinction from dust and because they are dominated by light from an older cooler stellar population that is more evenly distributed dynamically and a better tracer of the stellar mass in the galaxy than the bluer, hotter stars (e.g. Frogel 1988).

3. Morphology of the galaxy as compared to NGC 4314

We decompose the surface brightness at J band (and subsequently the potential) into its Fourier components in concentric annuli (e.g. Elmegreen et al. 1989). In Figure 1 we show these components given by $S(r,\theta) = S_0(r) + \sum_{m>0} S_{mc}(r)\cos(m\theta) + S_{ms}(r)\sin(m\theta)$ where $S(r,\theta)$ is the galaxy surface brightness. Fourier components of the potential in the plane of the galaxy, similarly defined, are shown in Figure 2. NGC 4314 has a stronger bar than NGC 1073 in the sense that the maximum of S_2/S_0 reaches 0.9 in NGC 4314 but only 0.7 in NGC 1073.

The knobby features (density enhancements) at the ends of the bar in NGC 4314 can be seen as strong higher order magnitude (S_4 and S_6) Fourier components that peak near the knobby features. In NGC 4314 the S_4 and S_6 maxima are 0.7 and 0.5 times the S_2 maximum respectively, whereas in NGC 1073 the S_4 and S_6 maxima are only 0.5 and 0.3 times the S_2 maximum. Because the S_2 moment dominates in NGC 1073, the bar has a more elliptical appearance. In NGC 4314 the central $20''$ containing the bulge is almost round whereas the isophotes of NGC 1073 are elliptical even near the nucleus (see contour plots in Figure 3).

4. Estimating the potential

The gravitational potential in the plane of the galaxy was derived by convolving the J image of NGC 1073 with a function that depends on the vertical structure of the disk (Paper I). Before convolution stars were removed from the J image. The galaxy is assumed to be face on, since the axis ratio at large radii (~ 0.9) is close to one. The disk is assumed to have density $\propto \mathrm{sech}(z/h)$ (van der Kruit 1988) where z is the height above the plane of the galaxy following van der Kruit 1988. The resulting potential is insensitive to the choice of vertical function for functions such as sech, sech^2 and exponential with equivalent $\langle z^2 \rangle$ (Quillen 1996).

Periodic orbits in NGC 1073 were found by numerical integration as in Paper I. The orbits in the plane of the galaxy were integrated in a potential resulting from smooth polynomial fits to the even order moments of the potential. Components of the potential are shown in Figure 2 along with the polynomial fits to them. The curvature of Φ_0, the azimuthally averaged component of the potential, is far higher in NGC 4314 than NGC 1073 because of its bulge. NGC 1073 has a weaker Φ_2/Φ_0 maximum than NGC 4314 and the higher order Fourier maxima of NGC 1073 are also weaker than those of NGC 4314. This is not surprising since the higher order Fourier components of the surface brightness are also weaker in NGC 1073.

5. Bar pattern speed and vertical scale height

Periodic orbits found in NGC 1073 are displayed with a contour plot of the galaxy in Figures 3a and 3b. For comparison Figures 3c and 3d shows similar results for NGC 4314 from Paper I.

We display a rotation curve and the location of the resonances for NGC 1073 in Figure 4.

In Paper I we found that both the vertical scale height and the pattern speed of the bar could be determined by comparing the periodic orbits to the shape of the galaxy in the limit that most stars in the galaxy are in orbits that are nearly periodic. The bar pattern speed is determined from the location of a resonance that causes features observed in the galaxy, whereas the vertical scale height is determined from the ellipticity of the orbits at regions distant from resonances. Some iteration is required to estimate both parameters since the rotation curve which determines the location of resonances depends on the vertical scale height, and the ellipticity of the orbits depends on the bar pattern speed.

We find that the orbits have ellipticities similar to the galaxy for a vertical scale height $h = 4'' \pm 2$. We find a vertical scale height to exponential scale length ratio of $\sim 1/12$ using a disk exponential scale length of $50''$ (in I band Elmegreen & Elmegreen 1985). This ratio is consistent with infrared studies of edge on galaxies (Barnaby & Thronson 1992; Wainscoat et al. 1989).

NGC 1073 has no distinct features obviously related to a resonance such as the knobby features at the ends of the bar in NGC 4314 caused by the inner 4:1 Lindblad resonance, which allowed us to fix the pattern speed of the bar. However we find that the orbits of NGC 1073 correspond to the shape of the galaxy only for pattern speeds that placed the 4:1 resonance at the end of the bar. This is because lenticular shaped orbits that are strongly peaked along the bar major axis exist only within the 4:1 resonance.

For early-type, strongly-barred galaxies, corotation should be close to the end of the bar, as predicted theoretically by Contopoulos 1980 and others. Using a measurement of the bar pattern speed various studies have estimated the ratio of the corotation radius to the bar semi-major axis in early-type galaxies. Kent 1990 found that this ratio was ~ 1.2 and later studies have confirmed this finding ratios of 1.2 ± 0.2 (Athanassoula 1992b) and 1.3 ± 0.1 (Elmegreen et al. 1996). In particular Elmegreen et al. 1996 noted that bars in early-type galaxies ended between the 4:1 resonance and the corotation radius but did not associate the end of the bar with any particular resonance. Because the 4:1 resonance is near the corotation radius in early-type galaxies it is difficult to clearly associate the end of the bar with the 4:1 resonance, though we noted in Paper I that in NGC 4314 the 4:1 resonance caused the knobby features at the end of the bar, and was coincident with the radius at which the isophotes began to twist. However in late-type galaxies the distance between the 4:1 resonance and the corotation radius is significantly larger than in early-type galaxies because of the shallower slope of the rotation curve. This makes it possible in NGC 1073 to clearly associate the end of the bar with the 4:1 resonance. That an exponential late-type bar also ends near the 4:1 resonance (well before corotation) is unexpected. We conjecture that a large class of bars end near this resonance.

The azimuthally averaged component of the potential gives a rotation curve (see Figure 4) for NGC 1073 which rises slowly and peaks past the end of the bar, not untypical for a late-type galaxy, whereas the rotation curve of NGC 4314 peaks near the end of its bar (see Figure 5 of

Paper I). We derive a maximum circular velocity of 160 km/s assuming a distance of 16Mpc (with a Hubble constant of 75 km/s Mpc) and using a mass-to-light ratio of $M/L_J = 4.3$ in units of solar masses to solar J magnitudes where L_J is the luminosity in the J band. Using these quantities we find a bar angular rotation rate or pattern speed of $\Omega_b = 0.0237 \pm 0.005 \mathrm{Myr}^{-1}$.

Our pattern speed places the corotation radius at $\sim 85''$ which puts the radius of corotation at a distance of 1.7 times the bar semi-major axis, assuming that the bar ends at $\sim 50''$. At $\sim 50''$ the magnitude of the S_2 component of the surface density experiences a drop and begins to twist (see Figure 1). 1.7 is actually a lower bound for this ratio since dark matter, which was not taken into account in constructing the rotation curve, will cause the radius of corotation to be at an even larger radius. This ratio is significantly higher than that found for early-type bars such as NGC 4314 (1.0-1.4) (Athanassoula 1992b; Elmegreen et al. 1996). The larger distance between the end of the bar and the corotation radius in the late-type galaxy allows us to clearly associate the end of the bar with the 4:1 resonance.

We find that NGC 1073 does not have an inner Lindblad resonance (see Figure 4) which implies that the entire length of the bar lacks resonances (except for a possible weak 3:1). This causes many of the orbits within the bar to be quasiperiodic, described in phase space by tori about the periodic orbits shown in Figure 3. In the next section we discuss the morphology of orbits that are not periodic.

6. Limiting the stellar velocity dispersion

In the previous section we have used the resemblance of the periodic orbits to the shape of the galaxy to determine the pattern speed and the scale height of the disk in the limit that all orbits are nearly periodic. To investigate the role of the stellar velocity dispersion in the plane of the galaxy we have integrated orbits near the periodic orbits (shown in Figure 3). Some non-periodic orbits are displayed in Figure 5 for NGC 1073 and in Figure 6 for NGC 4314. These figures show groups of orbits with identical initial positions but with varying initial velocities.

The stellar velocity dispersion can be defined locally in terms of a velocity dispersion ellipsoid. Pfenniger 1984 described the local velocity dispersion in terms of a sum of a dispersion from individual orbits, and that from the sum of all the orbits. By comparing Figures 5 and 6 showing the non-periodic orbits to Figure 3 showing the galaxy isophotes we can see that most stars in these galaxies must be in orbits that are close to being periodic. The velocity dispersion cannot be too high in NGC 4314 otherwise the knobby features observed at the ends of the bars could not exist. Likewise the strongly peaked top of the bar in NGC 1073 could not be sustained if the velocity dispersion were high. This enables us to place a limit on the velocity dispersion in both galaxies.

The second orbit from the bottom in Figure 5a and the same in Figure 6b were used to compute velocity dispersion ellipsoids at various locations in the orbit. Having a large percentage

of stars in orbits near to these orbits would not cause the galaxy to have a shape different than observed, however stars in orbits with larger velocity dispersions could not be represented in large numbers otherwise the galaxies could not have the fine structure observed.

We computed velocity dispersion ellipsoids in wedges centered at different position angles by considering all points in an orbit that were within an angular distance of 0.2 radians from the center of the wedge. Since these points cover a range of radius, this should be a reasonable estimate for the contribution to the dispersion from similar orbits at smaller and larger average radius. The largest component of the velocity dispersion ellipsoid occurs at the apocenters of the orbit where the ellipsoid is aligned in the radial direction. We find that the largest components of the the diagonalized velocity dispersion ellipsoid matrices are $(65\mathrm{km/s})^2$ and $(50\mathrm{km/s})^2$ in NGC 4314 and NGC 1073 respectively.

We note that outside the 4:1 resonance a significant number of stars could still be in orbits that cover a large area (e.g. Athanassoula et al. 1983; Contopoulos & Grosbøl 1989). In fact a large observed velocity dispersion is predicted at the end of the bar (Weinberg 1994).

We notice that the higher the initial velocity the rounder and larger the area covered by the orbit. Bars with larger velocity dispersion are expected to be rounder and more oval in shape. Because we have used the periodic orbit shapes to determine the vertical scale height, our estimate for the scale height is biased and is actually an overestimate. However we find that the size of the overestimate is smaller than the uncertainty in our value for the scale height itself. Likewise the initial assumption of a vertical scale height causes our limit on the velocity dispersion to be slightly underestimated. We note that by not including stars on ergodic orbits we have also underestimated this limit.

The orbits are bounded in extent by contours of an effective potential. In a system with a constant pattern speed the Jacobi integral given by

$$J = \Phi - \frac{1}{2}\Omega_b^2 r^2 + \frac{1}{2}v^2$$

is a conserved quantity. An effective potential can be defined as

$$\Phi_{eff} \equiv \Phi - \frac{1}{2}\Omega_b^2 r^2.$$

A star with a value J for the Jacobi integral is therefore bounded by the contour $\Phi_{eff} = J$. Orbits with a given J value range from being periodic orbits to filling a region bounded by a contour of constant effective potential. In Figure 7 we show contours for the effective potential for both galaxies. By comparing Figures 5 and 6 to Figures 7a and 7b we can see that stars with larger initial velocities fill regions that are bounded by the contours of constant effective potential. Stars in these orbits can affect the outer isophotes of the bar causing it to be rectangular or lenticular in shape (Athanassoula et al. 1990, Athanassoula 1991). Because the amount of time a star spends in a particular region can vary, the projected density of an orbit may have a boxier or more lenticular shape than the area covered by the orbit (see Figures 5 and 6).

The contours of the effective potential are quite different for NGC 4314 and NGC 1073 (see Figure 7). The bar in NGC 4314 forms a deeper well since this galaxy is of an earlier type. Near corotation the two terms $\frac{1}{2}\Omega_b r^2$ and Φ are about the same magnitude. In NGC 1073, since corotation is located far outside the bar, the effective potential is rounder near corotation than in NGC 4314 and is affected by spiral arms. In NGC 4314 stars past the end of the bar or with a high velocity dispersion are are trapped within the deep contours of the effective potential and so can support the shape of the bar. In NGC 1073, however, stars past the bar or with a high velocity dispersion will not support the bar, but will cover a more circular region.

7. The major axis surface brightness profile

It is possible to construct the surface density image of a galaxy from the periodic orbits if its brightness profile along some axis is known. Consider an initially exponential disk in which a bar slowly forms. Stars initially on orbits that are approximately circular end up in orbits that are close to periodic orbits such as shown in Figure 3. The azimuthally averaged surface brightness for both NGC 4314 and NGC 1073 are approximately exponential and so could be consistent with these bars having formed from initially exponential disks.

For NGC 1073 the orbits are similar in shape. Distributing stars on periodic orbits with surface density decreasing exponentially as a function of radius causes the resulting galaxy to have exponential surface brightness profiles along all position angles (including the major and minor axes of the bar). However in NGC 4314 the periodic orbits become increasingly peaked along the bar near the 4:1 resonance. Orbits near the 4:1 resonance have much lower speeds at the ends of the bar which results in a higher surface brightness than that away from this resonance. An initially exponential disk would have a strong density enhancement with respect to the initial disk along the top of the bar. The strength of the density enhancement grows as the distance to the 4:1 resonance decreases, reaching a maximum near this resonance. This results in a flat surface brightness profile along the bar major axis.

This effect can also be seen by considering the extreme values in the periodic orbits within the 4:1 resonance. In Table 1 we show axis ratios, velocity contrasts and maximum curvatures for the periodic orbits shown in Figure 3. The axis ratio is computed as the minimum radius divided by the maximum radius in the orbit (r_{min}/r_{max}), the velocity contrast is computed as the maximum speed in the orbit divided by the minimum speed in the frame in which the bar is stationary (v_{min}/v_{max}), and the curvature we compute the dimensionless quantity $|x''y' - y''x'|r_{max}$ where $x' = dx/ds$, ds is distance along a segment of the orbit, and the other derivatives are defined similarly. This curvature, which is the inverse of the radius of curvature, is the same quantity as measured in Athanassoula 1992a.

As we can see from Table 1, the axis ratios in both galaxies decrease as a function of radius, but rate of decrease is higher in NGC 1073. Athanassoula 1992a found that there is a stronger

variation in the axis ratio as a function of radius for bars with large Lagrangian radii (same as low pattern speeds), and for galaxies with larger bulges. Although NGC 1073 has a larger Lagrange radius with respect to the end of the bar than NGC 4314 it also has a smaller bulge.

A high velocity contrast in the orbit causes the surface brightness along the bar to increase compared to the azimuthally averaged value. This follows from conservation of mass in a steady state system. NGC 1073 has a slight decrease in the velocity contrast with increasing radius, whereas NGC 4314 has a slight increase which would increase the surface brightness along the bar major axis.

A high curvature at the end of the orbits also increases the surface brightness directly along the major axis of the bar. The curvature of the ends of the orbits in NGC 1073 does not vary much as a function of bar semi-major axis, though it is quite high. However even at a semimajor axis of $50''$, the curvature of the ends of the orbits in NGC 4314 is almost twice that at $30''$ and at a major axis of $55''$ it is four times that at $30''$. So NGC 4314 has a large increase in curvature near the 4:1 resonance. Because we also see an increase in the curvature at the $50''$ orbit the effect of the 4:1 resonance is stronger and extends over a larger radius in NGC 4314 than in NGC 1073. The combined effect of the increasing velocity contrast and curvature with increasing bar semi-major axis causes the surface brightness along the bar to be higher than the azimuthally averaged value and so is responsible for the flat bar profile shape and knobby features observed at the ends of the bar in NGC 4314 (see Figure 3d).

8. Summary and Discussion

In this paper we have compared orbits in the exponential late-type barred NGC 1073 and the earlier type flat-type barred galaxy NGC 4314. We find that the bar in both galaxies end near the inner 4:1 Lindblad (or ultraharmonic) resonance. In NGC 1073 the ratio of the radius of the end of the bar to the corotation radius is ~ 1.7 significantly longer than that found for early-type bars such as NGC 4314 (1.2-1.4) (Elmegreen et al. 1996). We find no inner Lindblad resonance in NGC 1073 so that the length of the bar is resonance free. By comparing the shapes of non-periodic orbits with the appearance of the galaxy we find that the bulk of the stars in both galaxies must be in orbits nearby to periodic orbits of the x_1 family. We place limits of $(65\mathrm{km/s})^2$ and $(50\mathrm{km/s})^2$ on the components of the diagonalized velocity dispersion ellipsoid matrix for stars in the bars of NGC 4314 and NGC 1073 respectively. These low values suggests that these bars formed and evolve by non-violent processes.

Both NGC 1073 and the early-type galaxy NGC 4314 have surface brightness profiles along the major axis that are consistent with their bars forming from an initially exponential disk. The strong 4:1 resonance and highly peaked orbits near this resonance in NGC 4314 cause the large density enhancement along the bar which results in a flat bar major axis surface brightness profile. A weaker 4:1 resonance and orbits that are similar to one another in NGC 1073 result in

exponential profiles along all position angles.

That both an exponential late-type bar (NGC 1073) and early-type bars end near the 4:1 Lindblad resonance is unexpected. One possible reason for this is that asymmetric terms in the potential cause the x_1 family past the 4:1 resonance to be highly asymmetric (Patsis et al. 1996a,b). In Paper I we noted that spiral structure, causing NGC 4314 to be asymmetric, begins at the location of the 4:1 resonance. The same is true in NGC 1073. We conjecture that many strong and slowly evolving bars end near this resonance independent of Hubble type. Since spiral arms can begin and end near their inner and outer 4:1 resonances (Patsis et al. 1994) this may facilitate the driving of spiral arms by bars in early-type galaxies (which have strong 4:1 resonances) and possibly explain why later type barred galaxies have weaker spiral arm patterns (Elmegreen et al. 1996). In early-type galaxies the spiral arm pattern could therefore exist with the same pattern speed as the bar, extend inside and outside the corotation radius and have a dust lane which crosses the spiral arm at corotation.

The stellar velocity dispersion in the bar should depend upon how the bar was formed. This means that our limit for the velocity dispersion in these galaxies could be used to constrain the timescale for bar formation. This timescale depends strongly on the dark matter content and bulge size in the galaxy (Athanassoula & Sellwood 1986) so that limiting the timescale for the formation of the bar could also be used to constrain the dark matter content in the central regions of galaxies.

The Schwarzschild method could be used on galaxy images to more carefully constrain the form of the stellar distribution function. This would give unbiased estimates of the bar pattern speed and the vertical scale height as well as make predictions for stellar velocity profiles in the bar that could be observed with a high resolution spectrograph. In this paper we have only considered orbits in the plane of the galaxy, but using the Schwarzschild method a self consistent three dimensional system could be studied.

We note that because of the large angular pixel scale of our images they were spatially undersampled. Higher resolution images should show more structure in these bars and will more tightly constrain the velocity dispersion.

Both galaxies studied here appear to have a low velocity dispersion for the bulk of the stars within the bar. This suggests that the difference in morphology of the two bars depends on the shape of the rotation curve or the Hubble type. We would then expect that earlier type galaxies have even stronger 4:1 resonances and stronger knobby features at the ends of their bars. Shorter bars should also have stronger knobby features. We expect that the ratio of the S_4 and higher order components to the S_2 component of the surface brightness should depend upon Hubble type and bar length with larger values for earlier Hubble types and shorter bars. Alternatively prominant knobby ends may only develop in bars that are evolving slowly. Then the ratio of the S_4 to the S_2 components would anticorrelate with other phenomena associated with faster evolution such as strong spiral structure, and assymetries in the bar and spiral arms. In this case strong

knobby features are commonly seen in early-type galaxies because their bars would be changing shape less rapidly than those in late-type galaxies. Bars which deviate from these patterns may be strongly influenced by gas dynamics or have large velocity dispersions.

Because of the strong higher order components in early-type barred galaxies, all the higher order resonances are strong. Vertical and planar stellar heating (increase in velocity dispersion) should be more efficient in these galaxies than in later type galaxies. This suggests that the rate that bars evolve, disks thicken and bulges grow could all be higher in earlier type barred galaxies than in late-type ones.

I acknowledge many helpful sujestions and criticisms from E. Athanassoula. I also acknowledge helpful discussions and correspondence with B. Elmegreen, D. Elmegreen and A. Gould. This paper was inspired by a talk given by D. Elmegreen at the Barred Galaxy meeting, May 1995, in Tuscaloosa. The OSU galaxy survey is being supported in part by NSF grant AST 92-17716. OSIRIS was built with substantial aid from NSF grants AST 90-16112 and AST 92-18449. A.C.Q. acknowledges the support of a Columbus fellowship and a grant for visitors from L'Observatoire de Marseille.

REFERENCES

Athanassoula, E., Morin, S., Wozniak, H., Puy, D., Pierce, M. J., Lombard, J., & Bosma, A. 1990, MNRAS, 245, 130

Athanassoula, E., Bienayme, O., Martinet, L., & Pfenniger, D. 1983, A&A, 127, 349

Athanassoula, E., & Sellwood, J. A. 1986, MNRAS, 221, 213

Athanassoula, E. 1991, in "Dynamics of Disk Galaxies", ed. B. Sundelius, Göteborg, Sweden, 149

Athanassoula, E. 1992a, MNRAS, 259, 328

Athanassoula, E. 1992b, MNRAS, 259, 345

Barnaby, D., & Thronson, M. A. 1992, AJ, 103, 41.

Contopoulos, G. 1980, A&A, 81, 198

Contopoulos, G., & Grosbøl, P. 1989, Astronomy and Astrophysics Review, 1, 261

DePoy, D. L., Atwood, B., Byard, P., Frogel, J., & O'Brien, T. 1993, In SPIE Vol 1946, Infrared Detectors and Instrumentation, p. 667

Elmegreen, B. G., & Elmegreen D. M. 1985, ApJ 288, 438

Elmegreen, B. G., Elmegreen, D. M., Chromey, F. R., Hasselbacher, D. A. & Bissell, B. A. 1996, AJ, in press

Elmegreen, B., Elmegreen, D. & Montenegro, L. 1989, ApJ, 343, 602

Frogel, J. A. 1988, ARA&A, 26, 51

Kent, S. M. 1990, AJ, 100, 377

Kent, S. M., & Glaudell, G. 1989, AJ, 98, 1588

Quillen, A. C., Frogel, J. A. & González, R. A. 1994, ApJ, 437, 162 (Paper I)

Quillen, A. C., Frogel, J. A., Kenney, J. D, Pogge, R. W., & DePoy, D. L. 1995, ApJ, 441, 549

Quillen, A. C. 1996, page 157 "Spiral galaxies in the Near-IR", Proceedings of the ESO-MPA Workshop Held at Garching, Germany 7-9 June 1995, eds D. Minniti and H.-W Rix, Springer-Verlag Berlin Heidelberg

Patsis, P. A., Hiotelis, N., Contopoulos, G. & Grosbøl, P. 1994, A&A, 286, 46

Patsis, P. A, Athanassoula, E., & Quillen, A. C. 1996a, page 246, "Spiral galaxies in the Near-IR", Proceedings of the ESO-MPA Workshop Held at Garching, Germany 7-9 June 1995, eds D. Minniti and H.-W Rix, Springer-Verlag Berlin Heidelberg

Patsis, P. A, Athanassoula, E., & Quillen, A. C. 1996b in preparation

Pfenniger, D. 1984, A&A, 141, 171

Pogge, R. W., Quillen, A. C., DePoy, D. L., Frogel, J. A., Terndrup, D., Sellgren, K., Ramírez, S. V., Houdashelt, M., Tiede, G., Ali, B. Kuchinski, L., Davies, R., Canzian, B. 1996, in preparation

Schwartzschild, M. 1979, ApJ, 232, 236

Sellwood, J. A., & Wilkinson, A. 1993, Rep. Prog. Phys., 56, 173

Sellwood, J. A. 1996, Barred Galaxies, IAU Colloquium No 157, ed. R. Buta, D. A. Crocker & B. G. Elmegreen, Astronomy Society of the Pacific, San Fransisco CA, 1996

van der Kruit, P. C. 1988, A&A, 192, 117

Weinberg, M. D. 1994, ApJ, 420, 597

Wainscoat, R. J., Freeman, K. C., & Hyland, A. R. 1989, ApJ, 337, 163

Fig. 1.— The Fourier components of the J surface brightness of NGC 1073. S_0 is the azimuthally averaged component in mag/arcsec^2. The $m = 2, 4$ and 6 components are given divided by S_0. For these components the solid triangles show show the cosine components and open squares show the sine components.

Fig. 2.— The Fourier components of the potential of NGC 1073. Φ_0 is the azimuthally averaged component in (km/s)^2 for distance and mass-to-light ratio given in the text. The $m = 2, 4$ and 6 components are given divided by Φ_0. For these components the solid triangles show show the cosine components and open squares show the sine components. Polynomial fits to these functions are shown as solid lines.

Fig. 3.— a) Prograde stellar orbits in NGC 1073 for a corotation radius at $r = 85''$ in the frame in which the bar is stationary. Points are plotted at equal time intervals in a single orbit. The density of the galaxy should increase where the velocity decreases. b) Contour plot of NGC 1073 of J surface brightness. The lowest contour is at a level 21.13 mag/"^{2}. The difference between the first five contours is equal to the surface brightness which corresponds to the magnitude of the lowest contour. c) Prograde stellar orbits in NGC 4314 for a corotation radius at $r = 70''$. d) Contour plot of NGC 4314 of K surface brightness. The lowest contour is at a level of 19.45 magnitudes per arcsec^2. The difference between contours is equal to the surface brightness which corresponds to the magnitude of the lowest contour. From Quillen et al. (1994).

Fig. 4.— a) Angular rotation rate for NGC 1073 $\Omega = v_c/r$ for v_c the circular rotation speed is plotted as the solid line and is derived from the azimuthally symmetric component of the potential $r\Omega^2 = d\Phi_0/dr$. Ω is given in Myr^{-1} for the mass-to-light ratio and distance given in the text. As an aid to finding the resonances, we have also plotted $\Omega - \kappa/2$ and $\Omega - \kappa/4$ as dotted lines where κ is the epicyclic frequency. For a bar angular rotation rate (shown as a horizontal dashed line) such that the corotation radius is at $r = 85''$, the inner 4:1 Lindblad resonance is at $r \sim 45''$ and there is no Inner Lindblad Resonance. b) Circular rotation speed v_c in km/s.

Fig. 5.— Non-periodic orbits in NGC 1073. Each column shows orbits with the same initial position as the periodic orbit shown in the bottom panel but with varying initial tangential velocities. The initial radius is a) $30''$ and b) $50''$.

Fig. 6.— Non-periodic orbits in NGC 4314. Each column shows orbits with the same initial position as the periodic orbit shown in the bottom panel but with varying initial tangential velocities. The initial radius is a) $40''$, b) $50''$ and c) $65''$.

Fig. 7.— Effective potentials for a) NGC 1073 and b) NGC 4314 for bar pattern speeds given in the text. The difference between contour levels is 2.5×10^3 $(\mathrm{km/s})^2$ for NGC 1073 and twice this for NGC 4314. Since the corotation radius for NGC 1073 is much greater than its bar length the potential is rounder near the Lagrange radius than in NGC 4314. Near the Lagrange radius in NGC 1073 structure from the spiral arms can be seen (compare to Figure 3b).

Table 1. Properties of Periodic Orbits

Galaxy	r_{max}	$\frac{r_{max}}{r_{min}}$	$\frac{v_{max}}{v_{min}}$	Curvature$_{max}$
NGC 4314	$30''$	2.94	6.22	12.9
NGC 4314	$40''$	2.66	5.55	14.3
NGC 4314	$50''$	2.50	6.79	20.9
NGC 4314	$55''$	2.42	10.7	51.9
NGC 1073	$20''$	3.49	10.2	22.2
NGC 1073	$30''$	2.80	7.84	17.4
NGC 1073	$40''$	2.14	4.69	19.8
NGC 1073	$50''$	1.70	5.25	26.9

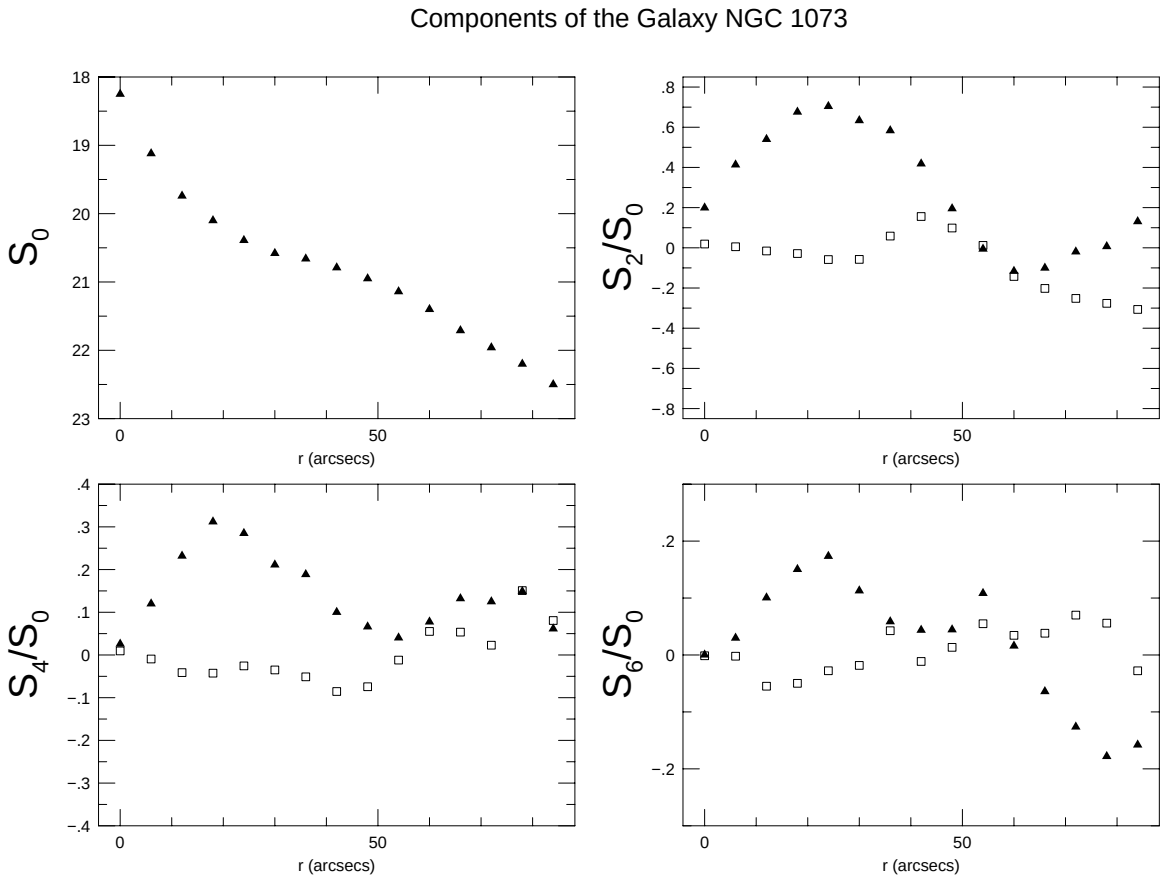

Fig. 1.— The Fourier components of the J surface brightness of NGC 1073. S_0 is the azimuthally averaged component in mag/arcsec^2. The $m = 2, 4$ and 6 components are given divided by S_0. For these components the solid triangles show show the cosine components and open squares show the sine components.

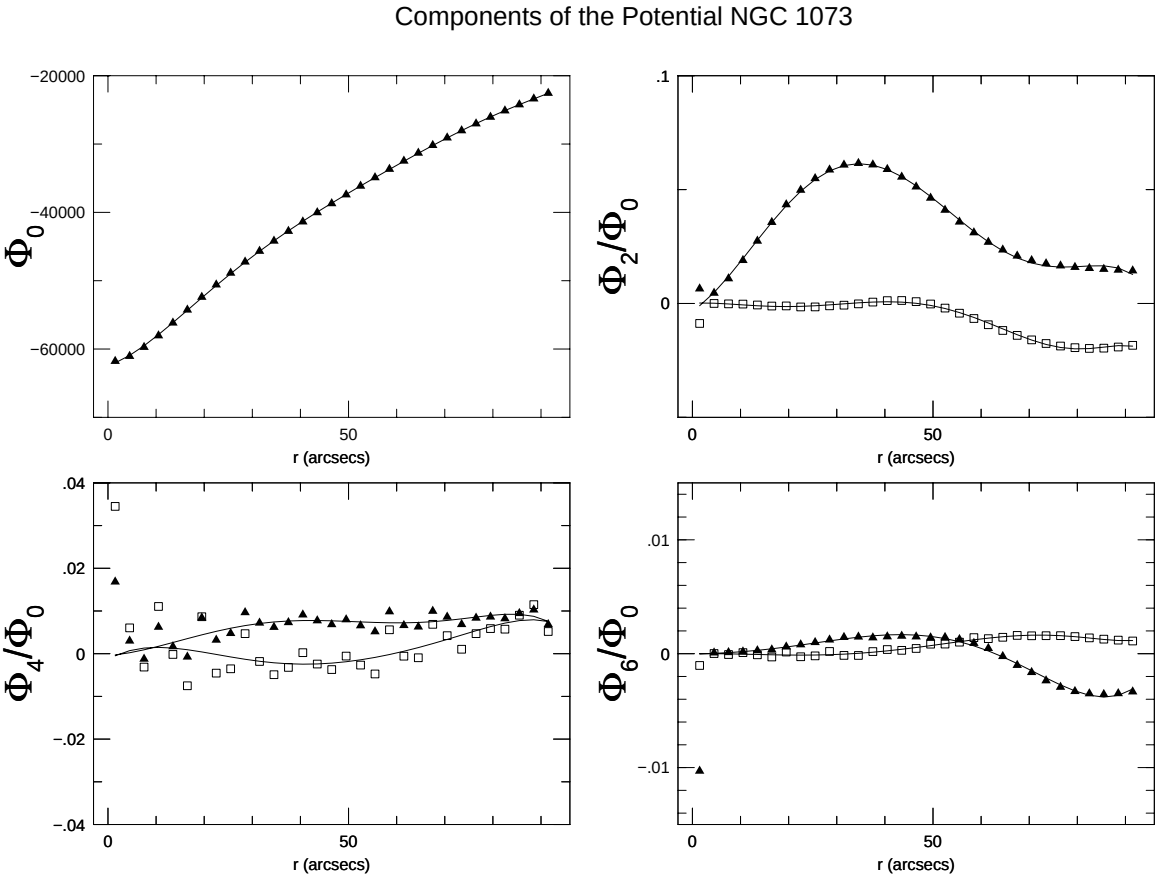

Fig. 2.— The Fourier components of the potential of NGC 1073. Φ_0 is the azimuthally averaged component in $(\mathrm{km/s})^2$ for distance and mass-to-light ratio given in the text. The $m = 2, 4$ and 6 components are given divided by Φ_0. For these components the solid triangles show show the cosine components and open squares show the sine components. Polynomial fits to these functions are shown as solid lines.

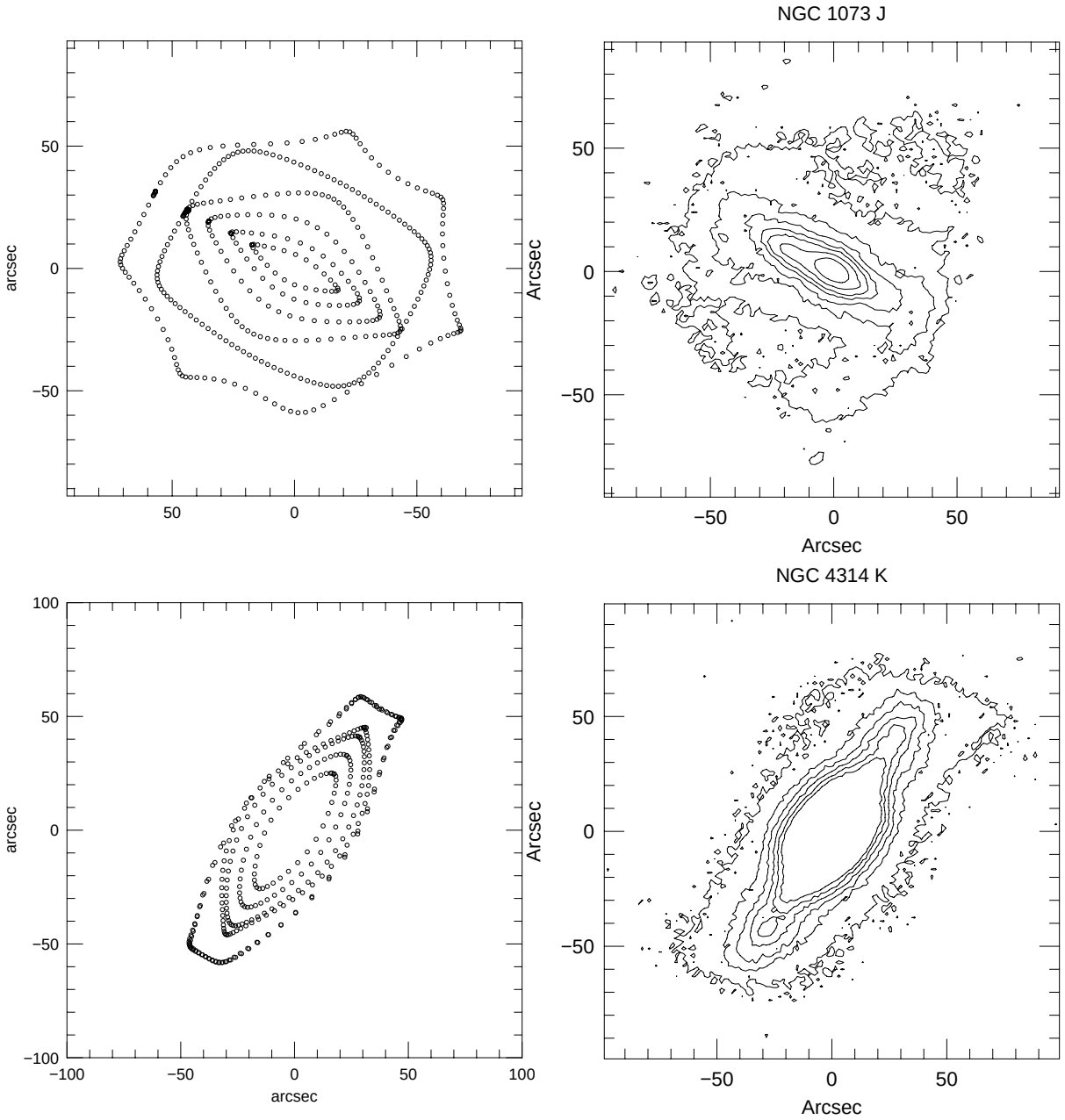

Fig. 3.— a) Prograde stellar orbits in NGC 1073 for a corotation radius at $r = 85''$ in the frame in which the bar is stationary. Points are plotted at equal time intervals in a single orbit. The density of the galaxy should increase where the velocity decreases. b) Contour plot of NGC 1073 of J surface brightness. The lowest contour is at a level 21.13 mag/"^{2}. The difference between the first five contours is equal to the surface brightness which corresponds to the magnitude of the lowest contour. c) Prograde stellar orbits in NGC 4314 for a corotation radius at $r = 70''$. d) Contour plot of NGC 4314 of K surface brightness. The lowest contour is at a level of 19.45 magnitudes per arcsec^2. The difference between contours is equal to the surface brightness which corresponds to the magnitude of the lowest contour. From Quillen et al. (1994).

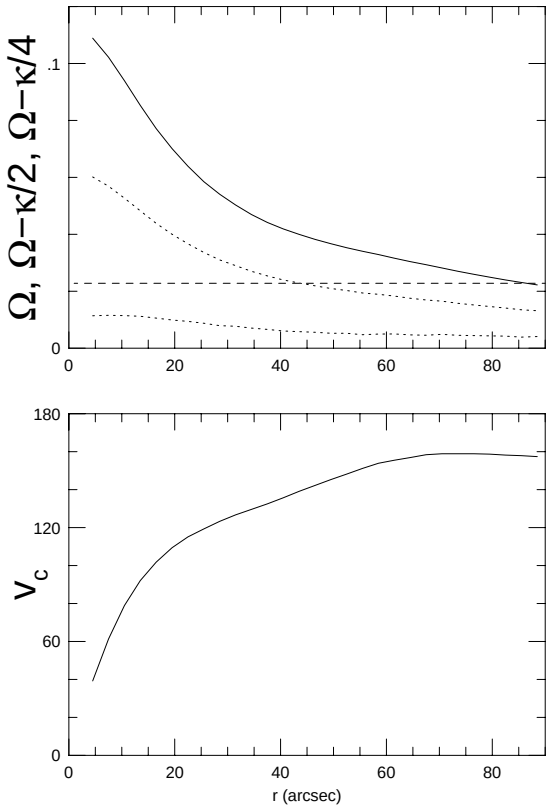

Fig. 4.— a) Angular rotation rate for NGC 1073 $\Omega = v_c/r$ for v_c the circular rotation speed is plotted as the solid line and is derived from the azimuthally symmetric component of the potential $r\Omega^2 = d\Phi_0/dr$. Ω is given in Myr^{-1} for the mass-to-light ratio and distance given in the text. As an aid to finding the resonances, we have also plotted $\Omega - \kappa/2$ and $\Omega - \kappa/4$ as dotted lines where κ is the epicyclic frequency. For a bar angular rotation rate (shown as a horizontal dashed line) such that the corotation radius is at $r = 85''$, the inner 4:1 Lindblad resonance is at $r \sim 45''$ and there is no Inner Lindblad Resonance. b) Circular rotation speed v_c in km/s.

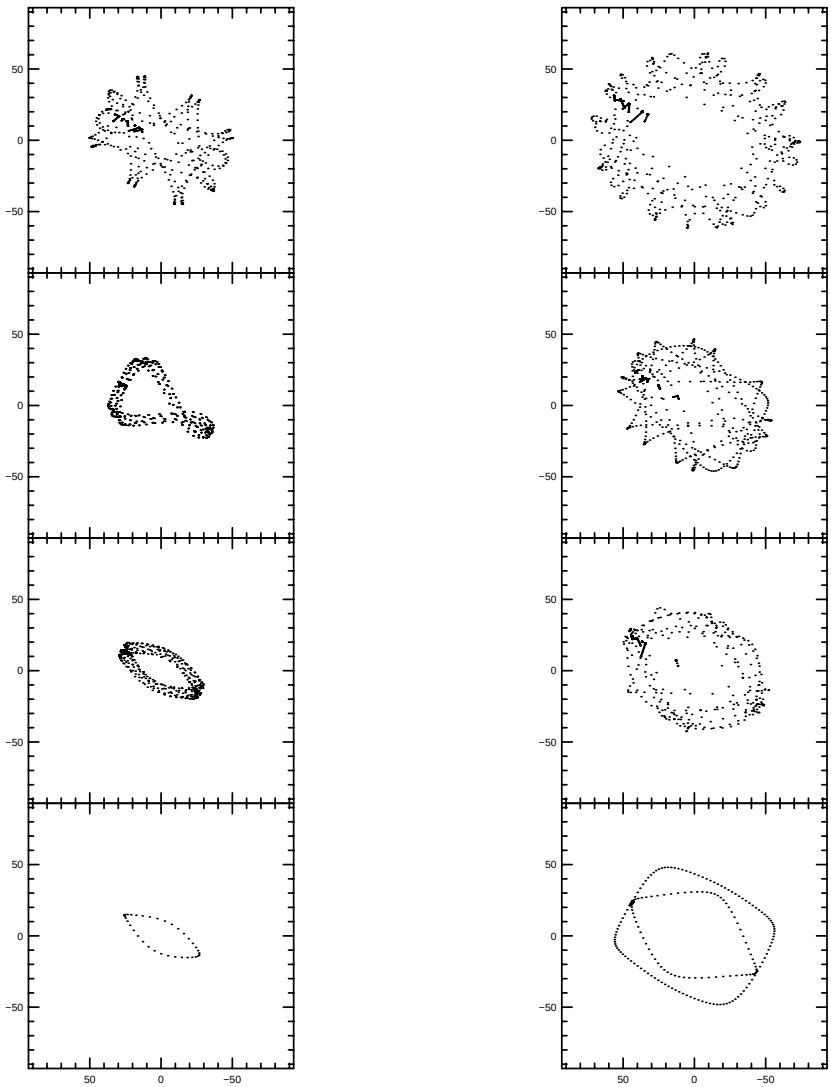

Fig. 5.— Non-periodic orbits in NGC 1073. Each column shows orbits with the same initial position as the periodic orbit shown in the bottom panel but with varying initial tangential velocities. The initial radius is a) 30″ and b) 50″.

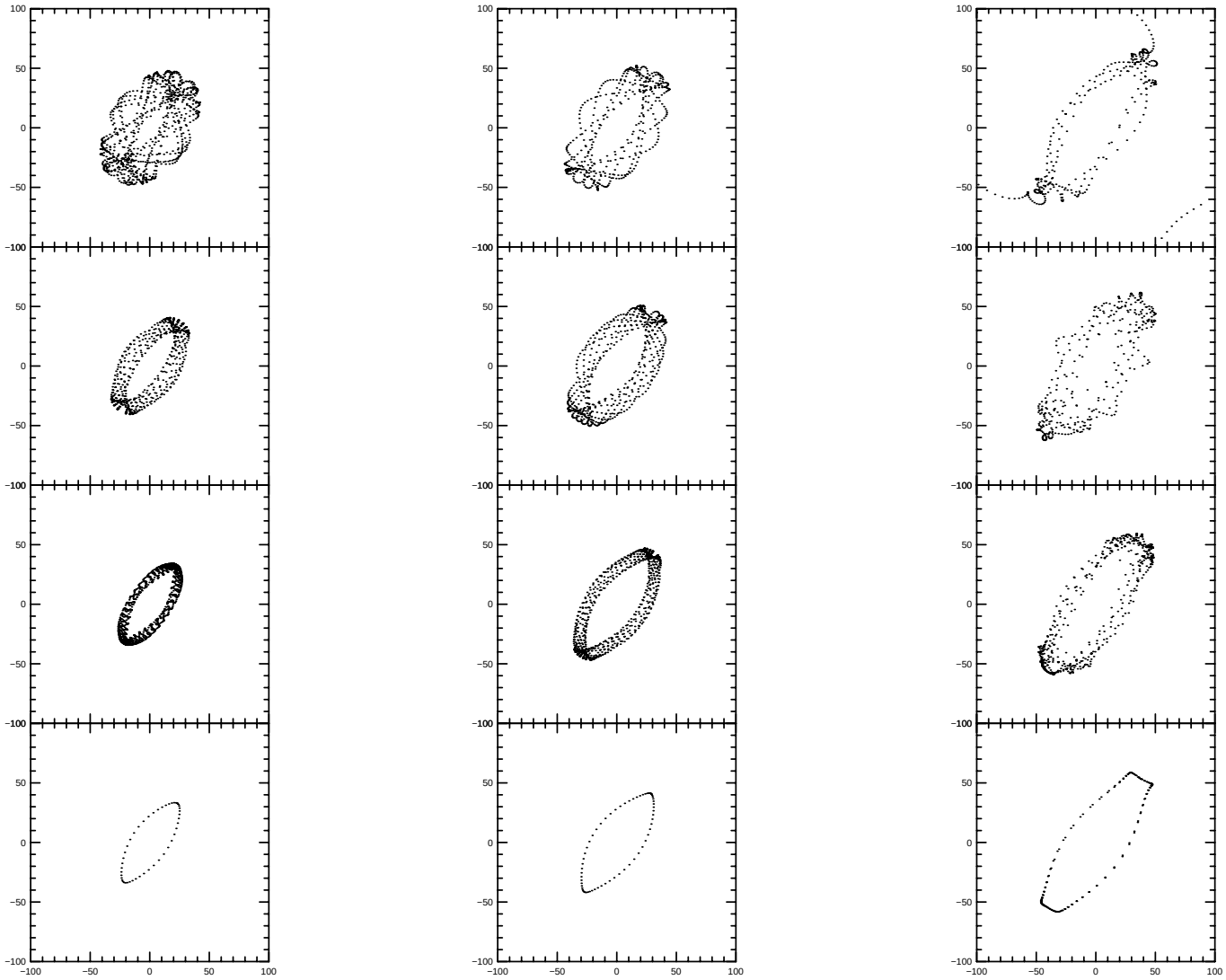

Fig. 6.— Non-periodic orbits in NGC 4314. Each column shows orbits with the same initial position as the periodic orbit shown in the bottom panel but with varying initial tangential velocities. The initial radius is a) 40″, b) 50″ and c) 65″.

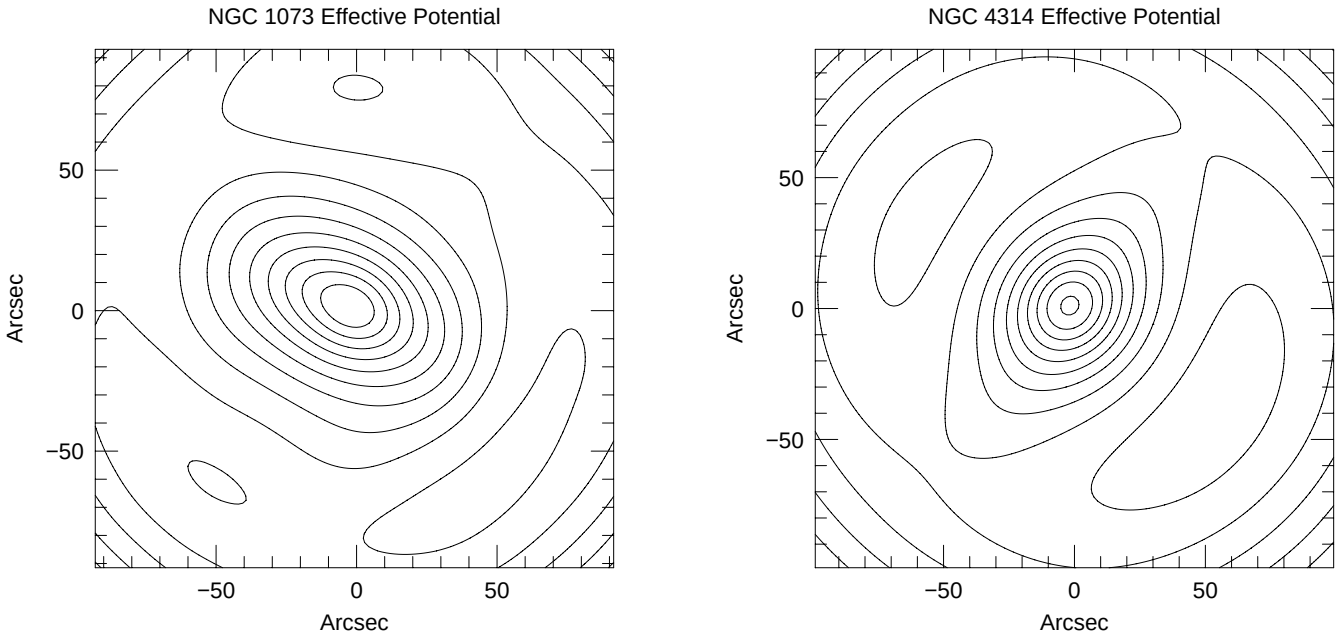

Fig. 7.— Effective potentials for a) NGC 1073 and b) NGC 4314 for bar pattern speeds given in the text. The difference between contour levels is 2.5×10^3 $(\mathrm{km/s})^2$ for NGC 1073 and twice this for NGC 4314. Since the corotation radius for NGC 1073 is much greater than its bar length the potential is rounder near the Lagrange radius than in NGC 4314. Near the Lagrange radius in NGC 1073 structure from the spiral arms can be seen (compare to Figure 3b).